

A Quantum Optimization Case Study for a Transport Robot Scheduling Problem

Dominik Leib^{1*}, Tobias Seidel¹, Sven Jäger¹, Raoul Heese¹, Caitlin Jones²,
Abhishek Awasthi^{2†}, Astrid Niederle³, Michael Bortz¹

¹ Fraunhofer ITWM, Kaiserslautern, Germany

² BASF Digital Solutions GmbH, Ludwigshafen am Rhein, Germany

³ BASF SE, Ludwigshafen am Rhein, Germany

Abstract

We present a comprehensive case study comparing the performance of D-Waves’ quantum-classical hybrid framework, Fujitsu’s quantum-inspired digital annealer, and Gurobi’s state-of-the-art classical solver in solving a transport robot scheduling problem. This problem originates from an industrially relevant real-world scenario. We provide three different models for our problem following different design philosophies. In our benchmark, we focus on the solution quality and end-to-end runtime of different model and solver combinations. We find promising results for the digital annealer and some opportunities for the hybrid quantum annealer in direct comparison with Gurobi. Our study provides insights into the workflow for solving an application-oriented optimization problem with different strategies, and can be useful for evaluating the strengths and weaknesses of different approaches.

Keywords— Optimization, Quantum Computing, Robot Scheduling

1 Introduction

Quantum computing (QC) is a field that has witnessed a rapid increase in interest and development over the past few decades since it was theoretically shown that quantum computers can provide an exponential speedup for certain tasks (Deutsch, Jozsa 1992; Grover 1996; Shor 1994). Translating this potential into a practically relevant quantum advantage, however, has proven to be a very challenging endeavor. Nevertheless, the emerging field is considered to have a highly disruptive potential for many domains, for example in machine learning (Schuld, Sinayskiy, Petruccione 2015), chemical simulations (Cao *et al.* 2019) and optimization (Li *et al.* 2020), the domain of this work. Due to the fact that optimization problems are of utmost importance also for industrial applications, we investigated a potential advantage of quantum and quantum-inspired technology for the so-called *transport robot scheduling problem* (TRSP), a real-world use-case in optimization that is derived from an industrial application of an automatized robot in a high-throughput laboratory. The optimization task is to plan a time-efficient schedule for the robot’s movements as it transports chemical samples between a rack and multiple machines to conduct experiments. This is an NP-hard problem which for certain instances can be challenging to solve using classical computing techniques, and hence is an attractive candidate to search for an advantage with non-classical techniques.

*D. Leib: dominik.leib@itwm.fraunhofer.de

†A. Awasthi: abhishek.awasthi@basf.com

In our study, we compared the solution quality and runtime of different solvers on a large set of instances of the problem. As solvers, we considered D-Wave’s hybrid *Leap* framework (LBQM) that makes use of the D-Wave quantum annealer (D-Wave Systems Inc. 2020), Fujitsu’s digital annealer (FDA)(Nakayama *et al.* 2021), Fujitsu’s digital annealer hybrid framework (FDAh), as well as the industry-grade Gurobi solver (Gurobi Optimization, LLC 2023). As a key element of this work, we provide three different models for the TRSP that follow different design philosophies. This is justified by the different ways in which the problem task can be modelled and the inherent differences in the problem formulations that the solvers addressed can accept. LBQM, FDA and FDAh are restricted to a formulation as a quadratic unconstrained binary optimization (QUBO), whereas a mixed integer program (MIP) with integer and float variables can be used by Gurobi, which makes a comparison of multiple formulations meaningful.

The TRSP considered in this paper is a special combination of different scheduling problems that, to our knowledge, has not been considered before. Scheduling problems have been studied intensively for several decades and classical algorithms exist for numerous variants (Brucker 2007; Pinedo 2016). Since most of the industry-relevant scheduling problems are NP-hard, these classical algorithms mainly consist of meta-heuristics or use general-purpose MIP solvers, which basically solve the problem using a branch and bound approach with several additional improvements like cutting planes. In addition to classical algorithmic developments, a considerable amount of research has also been done in hardware-based parallel computing, especially in general purpose computation on graphics processing unit (GPGPU) parallelization (Chakroun *et al.* 2013; Awasthi *et al.* 2016). The problem discussed in this work is an extension of the typical job shop scheduling problem (JSSP), where the inclusion of a robot adds additional restrictions. More specifically, the studied scheduling problem falls into the category of robotic cell scheduling and automated guided vehicles (AGV) scheduling problems. Most work on robotic cell scheduling deals with infinite cyclic schedules (Dawande *et al.* 2007). This comprises polynomial-time algorithms and hardness results (Steiner, Xue 2005), MIP techniques (Phillips, Unger 1976; Brucker, Burke, Groenemeyer 2012; Feng, Che 2013) and heuristic approaches (Liu, Kozan 2017). Many efficiently solvable and hard special cases have been identified (Shabtay, Arviv 2016) and heuristics have been proposed for some of the hard cases (Stern, Vitner 1990). Those problems differ from our use case in one way or another. The problems considered by the above-cited papers allow, unlike our use case, that the jobs can wait at a machine after their completion before being picked up by the robot. Robotic cell scheduling problems without this possibility have been studied by (Agnetais 2000; Agnetais, Pacciarelli 2000), whose problems differ from our, among others, in the considered objective function. Our objective function, the total job completion time, has been extensively studied for flow shop scheduling problems without a robot (Pinedo 2016; Hall, Sriskandarajah 1996; Allahverdi 2016; Röck 1984), the latter of which shows that the no-wait variant is strongly NP-hard on two machines. Apart from the no-wait constraint, the problem considered in our work is characterized by the fact that jobs have to go to the last machine several times. Such settings are known as a re-entrant flow shops, for which (Jing, Huang, Tang 2011) developed a heuristic algorithm.

We are mainly interested in the performance of non-standard solution approaches using quantum or quantum-inspired solvers in this study. Because these solvers rely on heuristics, benchmarks for real-world applications are a highly relevant research topic. Most quantum optimization approaches fall into two major groups, one for gate-based hardware and one for annealing-based hardware (Alexeev *et al.* 2021). The majority of gate-based approaches to optimization use parameterized gates to find the ground state of a Hamiltonian related to the cost function of the optimization problem in a quantum-classical hybrid fashion, for example via the quantum approximate optimization algorithm (QAOA) (Farhi, Goldstone, Gutmann 2014; Blekos *et al.* 2023).

Approaches based on quantum annealing also seek to find the ground state of a Hamiltonian, but by aiming for an adiabatic change from an initial state that can be easily prepared. In contrast to actual quantum computing devices, other classical software and hardware components are merely *inspired* by quantum computing, for example FDA (Aramon *et al.* 2019) and Toshiba’s Simulated Bifurcation Machine (TSB) (Tatsumura, Dixon, Goto 2019). Typically, optimization tasks for quantum solvers and the aforementioned quantum-inspired technologies are modeled as QUBO problems (Kochenberger *et al.* 2014). An in-depth analysis of pure QUBO comparison on four quantum and quantum-inspired solvers

can be found in (Oshiyama, Ohzeki 2022). In their work, the authors compare the solutions of a library of quadratic benchmark problems on the D-Wave quantum annealer, FDA, and TSB against each other.

QC has already been successfully used for optimization in various fields. For example, in (Mizuno, Komatsuzaki 2023), chemical reaction networks are optimized with quantum computing. In (Streif *et al.* 2021), it is shown that using the QAOA, it is possible to beat some classical heuristic algorithms on the binary paint shop problem. However, some work has shown that the current circuit model algorithms are not always adequate enough to reach significant convergence required for a good solution (Awasthi *et al.* 2023). Quantum annealing has proven to offer some advantage against the classical simulated annealing algorithm for a spin-glass problem, using D-Wave hardware (Raymond *et al.* 2023), but this is no conclusive evidence. In (Ebadi *et al.* 2022), the authors present a solution to the maximum independent set (MIS) problem using a Rydberg atom device, along with a claim of a possible super-linear quantum speed-up against classical simulated annealing. Other classical algorithms might still be superior to a quantum approach on current devices (Albash, Lidar 2018). Several works consider scheduling problems (Yarkoni *et al.* 2021; Carugno, Ferrari Dacrema, Cremonesi 2022; Tomasiewicz *et al.* 2020). In (Geitz *et al.* 2022), an AGV transportation problem using different classical and quantum approaches is studied and (Ikeda, Nakamura, Humble 2019) investigates a nurse scheduling problem with the usage of a quantum annealer.

The remaining manuscript is structured as follows. We provide a detailed description of the TRSP and its mathematical modeling in Section 2. In Section 3, we describe the design of our numerical study and list the problem instances and solvers that we use. The results of this study are presented in Section 4. Finally, we conclude our study in Section 5.

2 Transport Robot Scheduling Problem

In this section, we present a detailed explanation of the TRSP, which is a real-world use case derived from one of BASF’s high-throughput laboratories. This optimization problem is about finding the most time-efficient route of a transport robot tasked with moving chemical samples from one processing machine to another, as illustrated in Fig. 1. In the following, we first provide a general description of the problem setup and then present different modeling approaches. These models build the foundation of the subsequent benchmarks.

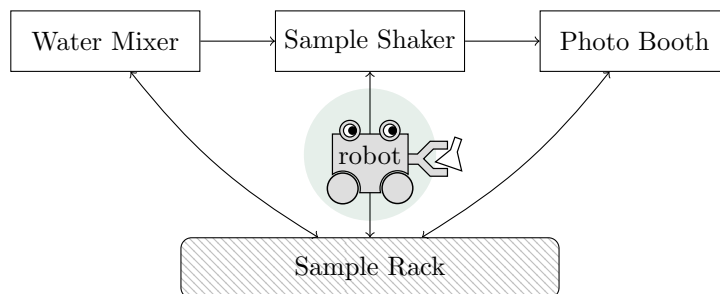


Figure 1: Sketch of the high-throughput laboratory setup for the TRSP. The laboratory consists of a sample rack and different processing machines (water mixer, sample shaker and photo booth). The arrows indicate how the samples may be transported by the robot between the machines and the rack, one at a time.

2.1 Problem Description

The laboratory we are modeling here consists of a *sample rack* and three different processing machines: a *water mixer*, a *sample shaker* and a *photo booth*. And, finally, the *robot* itself that is tasked with carrying chemical samples from one place to another with the goal to conduct chemical experiments.

Only the experimental plan (i. e., how each sample has to be processed in the laboratory) is predefined in advance, but not the specific order of the experiments. Initially, a certain number of samples is stored on the rack. Each of these samples needs to be first taken to the water mixer, then to the sample shaker. Once the sample shaking is completed, one or more photos have to be taken of each sample at the photo booth. Consecutive photos need to be taken after specific (i. e., predefined) time intervals, where the first photo of each sample has to be taken immediately after the shaking process. Finally, each sample has to be brought back to the rack. The processing times for different samples on the same machine can be different as specified by the experimental plan. We assume that each machine can only hold (and process) one single sample at any given time, or remain idle, and the processing steps cannot be interrupted before their completion. It is required that a machine starts processing a sample as soon as the sample is brought by the robot. Moreover, we assume that a sample has to be moved by the robot in-between two processing steps. Hence, a sample has to be lifted from a machine (and the machine is made available) as soon as it finishes processing.

By definition, the robot requires exactly one time unit to move from any place to any other, with or without a sample, and picking up or dropping a sample does not require extra time. Like the machines, the robot can transport only a single sample at any given time or drive empty or remain idle. In particular, it is not possible that the robot places a sample at a machine and picks up another at the same time.

The objective of this scheduling task is to minimize the *sum of sample completion times*, i. e., the sum of the times when the samples arrive at the rack after their last photo has been taken. The solution of this optimization problem is a sequence of tasks for the robot that yields an efficient laboratory operation.

2.2 Mathematical Modeling

In our benchmark, we test three modeling approaches against each other. On the quantum and quantum-inspired side we consider a QUBO formulation, whereas on the classical side we use two MIP formulations. First, a so-called *sequence model* and second, a so-called *time-indexed model*. In the following, we first introduce the common terminology for all modeling approaches. Next, we shortly sketch the main features of each model. For a more detailed description, we refer to Appendix A. The motivation for the development of multiple models is to carry out a comparison between the solutions obtained by the most suitable problem encoding for quantum and classical solvers. This ensures that we are comparing the best of both worlds (classical and quantum), and do not restrict ourselves to a model which is more suitable for quantum over classical computing.

2.2.1 Common Terminology

The processing machines are addressed by M_1 for the water mixer, M_2 for the sample shaker and M_3 for the photo booth. The scheduling time is discretized into time slots which all have length of one time unit. The transport robot takes one time unit for each operation that is either transportation or empty traversal between the machines and the rack. In this way, each transport robot scheduling problem is uniquely determined by the following parameters:

- The number of samples to be scheduled $N \geq 1$.
- The number of photos $K \geq 1$, which agrees for each sample $j \in \{1, \dots, N\}$.
- The processing times $p_{j,1}, p_{j,2}, p_{j,3} \in \mathbb{N}_{>0}$ for machines M_1, M_2 and M_3 , which can vary for each sample $j \in \{1, \dots, N\}$.
- The time gaps $g_{j,k} \in \mathbb{N}_{\geq 2}$ to be kept between consecutive photos k and $k+1$ for $k \in \{1, \dots, K-1\}$, which also can vary for each sample $j \in \{1, \dots, N\}$.

As an example, Fig. 2 provides a feasible schedule in form of a Gantt chart to visualize these parameters.

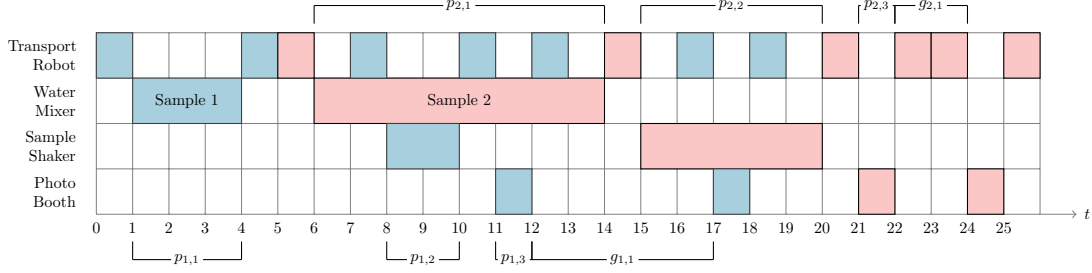


Figure 2: An example Gantt chart of a robot transport scheduling problem (as sketched in Fig. 1) with $N = 2$ samples and $K = 2$ photos. When a sample is processed on one of the machines or carried by the robot in the time-frame $[t, t']$, a bar is drawn from t to t' in the respective row in a corresponding color. Empty movements of the robot are not drawn explicitly. For example, at time $t = 13$ the robot is at the rack as sample 1 has been brought to the sample rack from $t = 12$ to 13 . It takes one unit of time for the robot to travel from the rack to the water mixer to pick up sample 2 at $t = 14$. From $t = 22$ to $t = 23$, the sample is brought from the photo booth to the rack and back, which is a consequence of the assumption that a sample has to be moved by the robot in-between two processing steps. The objective value of the depicted schedule is $19 + 26 = 45$.

2.2.2 QUBO Model

A general QUBO reads

$$\begin{aligned} \min_x \quad & x^\top \cdot Q \cdot x \\ \text{s.t.} \quad & x \in \{0, 1\}^n \end{aligned} \quad (1)$$

for some matrix $Q \in \mathbb{R}^{n \times n}$, where x represents a vector of n binary optimization variables. Two challenging properties of QUBOs must be taken into account in the modeling. Since only binary variables are allowed, this implies that other types of variables must be avoided, i. e. a reformulation into a binary form is necessary. Second, the problem is unconstrained. This restriction can be overcome by using *penalty terms*, which are quadratic functions in the model variables that evaluate to a positive value when the current assignment of values to the variables leads to an infeasible solution. Typically, the penalty terms are designed to yield 0 if the corresponding solution is feasible, so that they do not contribute to the objective values of feasible solutions. More general information about QUBOs and their properties can be found, e. g., in Ref.(Kochenberger *et al.* 2014; Lucas 2014; Glover, Kochenberger, Du 2018).

Our proposed QUBO model for the TRSP is based on the well-known starting time formulation (see e. g. Ref.(Carugno, Ferrari Dacrema, Cremonesi 2022)) and can be written as

$$\begin{aligned} \min_x \quad & \rho_0 F(x) + \sum_{i=1}^7 \rho_i P_i(x) \\ \text{s.t.} \quad & x \in \{0, 1\}^n, \end{aligned} \quad (2)$$

where F is the objective function and P_1, \dots, P_7 denote the penalty functions and $\rho_0, \dots, \rho_7 \in \mathbb{R}_{>0}$ are tunable parameters that have to be chosen such that the objective and penalty terms are suitably balanced. As in equation (1), n represents the total number of binary optimization variables. These have a distinct meaning that can be identified with three indices. Specifically,

$$x_{j,m,t} := \begin{cases} 1, & \text{if sample } j \text{ starts processing on machine } M_m \text{ at time } t, \\ 0, & \text{otherwise} \end{cases} \quad (3)$$

for all $j \in \{1, \dots, N\}$, $m \in \{1, 2, 3\}$ and $t \in \{1, \dots, T-1\}$. Here, T denotes the time horizon, which is chosen in such a way that there is enough time to schedule all samples sequentially, implying that

there is at least one feasible solution. It can be explicitly computed for each instance as described in Appendix A.1. In terms of Fig. 2, one has, for example, $x_{1,1,1} = 1$ and $x_{1,2,8} = 1$.

The penalty terms for the QUBO model have to be formulated using the binary optimization variables. This section only provides an example for such a term, a complete description can be found in Appendix A.1. Specifically, we consider here the constraint that each sample must access the machines M_1 and M_2 exactly once, which can be achieved by

$$P_1 := \sum_{j=1}^N \sum_{m=1}^2 \left[\left(\sum_{t=1}^{T-1} x_{j,m,t} \right) - 1 \right]^2. \quad (4)$$

This term evaluates to zero if and only if for each pair of sample j and machine M_m , the variable $x_{j,m,t}$ is 1 for precisely one time slot t . Since P_1 is bounded below by 0 due to its quadratic nature, each local minimum of P_1 is a feasible solution w.r.t. the rule of machine access to M_1 and M_2 . The other penalty terms can be formulated similarly.

Finally, the objective function F sums up for each sample the time when the sample arrives at the rack after the entire scheduling process ("sum of sample completion times"). For example, the objective function in the case of Fig. 2 evaluates to 45 time units.

2.2.3 MIP Models

A general MIP reads

$$\begin{aligned} \min_{x,y} \quad & c_1^\top x + c_2^\top y \\ \text{s.t.} \quad & A_1 x + A_2 y \leq b \\ & C_1 x + C_2 y = d \\ & x \in \mathbb{Z}^n, y \in \mathbb{R}^m, \end{aligned} \quad (5)$$

where $A_1 \in \mathbb{Z}^{k \times n}$, $C_1 \in \mathbb{Z}^{l \times n}$, $A_2 \in \mathbb{Z}^{k \times m}$, $C_2 \in \mathbb{Z}^{l \times m}$, $b \in \mathbb{Z}^k$, $d \in \mathbb{Z}^l$, $c_1 \in \mathbb{Z}^n$ and $c_2 \in \mathbb{Z}^m$ for $n, m, k, l \in \mathbb{N}_{>0}$. MIPs have been used since the late 1950s as a tool for solving scheduling problems. It is not possible to model the disjunctive constraints resulting from the discrete ordering decisions only by means of starting time variables. Different types of binary variables have been proposed to achieve this. The main types are position variables x_{ijk} indicating if job j is the k th job on machine i (Wagner 1959), linear ordering variables δ_{ijk} deciding if job j is processed before job k on machine i (Manne 1960) and time-indexed variables x_{ijt} specifying that job j is started (or processed or completed) on machine i at time t (Bowman 1959; Pritsker, Waiters, Wolfe 1969). Ref.(Ku, Beck 2016) compared these three approaches experimentally for a job shop scheduling problem.

Due to the powerful nature of (mixed) integer programming in contrast to the restrictive nature of the QUBO models, we provide two MIP models to be solved using Gurobi. The first one, in the following named *sequence model*, makes use of integer start time and binary linear ordering variables. The second model, called the *time-indexed model*, is restricted to a binary formulation comparable to the QUBO model, where we make use of time-indexed variables.

2.2.4 MIP: Sequence Model

In the sequence model, we model sequences of *events* that affect the behavior of the transport robot with respect to the machines and the photos of a sample. We define the *set of events* as

$$E := \{(j, i, a) \mid j \in \{1, \dots, N\}, i \in \{1, \dots, 2 + K\}, a \in \{0, 1\}\}. \quad (6)$$

An event $e = (j, i, 0)$ represents either that a sample j is placed on machine M_i for $i \in \{1, 2\}$ or to the $(i-2)$ th photo shoot for $i > 2$, an event $(j, i, 1)$ corresponds to picking it up again. For each event $e \in E$ we define an optimization variable $\tau_e \in \mathbb{R}_{\geq 0}$ to model the time for event e to happen. In terms of Fig. 2, we have, for example, $\tau_{(1,1,0)} = 1$ and $\tau_{(1,1,1)} = 4$. A simple formulation can be achieved by additionally introducing a binary variable for each pair $e, f \in E$, $e \neq f$ of events that indicates if e occurs before f . We reduce the size of the model by exploiting the fact that the ordering of some events is fixed

or coupled. For example, we do not need a variable that specifies the order in which a given sample is brought to the water mixer and to the sample shaker. This leads to three sets of linear ordering variables that can be found in Appendix A.2, as well as the various constraints to ensure feasibility. The objective function (i.e., the sum of the sample completion times) can be easily expressed using the variables τ_e corresponding to events when a sample is picked up from the last photo.

2.2.5 MIP: Time-Indexed Model

The second constrained model makes use of discrete time-indexed variables similar to the QUBO model from Appendix A.1. In this formulation, we model the behavior of the transport robot by defining certain routes a sample can be transported along, which include those from the rack to all machines and back or movements between subsequent machines. The numbering of the moves is shown in Fig. 3.

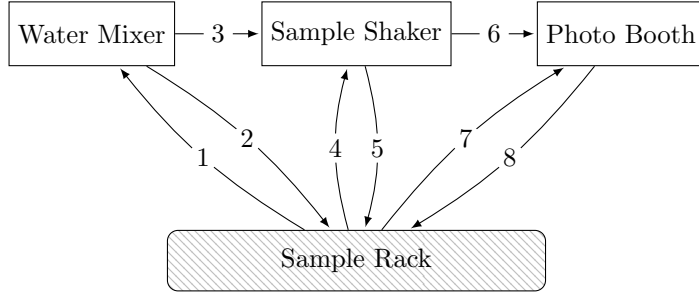


Figure 3: Numbering of the eight different routes the transport robot can move along between the machines and the rack as sketched in Fig. 1.

As the model name implies, we have, given a discrete time horizon $T \in \mathbb{N}_{>0}$, binary variables to model when each sample takes which route as

$$y_{j,r,t} := \begin{cases} 1, & \text{if sample } j \text{ is transported by the robot on route } r \text{ during the time } (t, t+1), \\ 0, & \text{otherwise} \end{cases} \quad (7)$$

for all $j \in \{1, \dots, N\}$, $r \in \{1, \dots, 8\}$ and $t \in \{0, \dots, T-1\}$. In terms of the Gantt chart from Fig. 2, this would imply $y_{1,1,0} = 1$, $y_{1,2,4} = 1$, $y_{2,1,5} = 1$ and so on. The time horizon T is defined as for the QUBO model, see equation (9).

The constraints of the model are similar to the penalty terms of the QUBO Model and are listed in Appendix A.3. The objective function (i.e., the sum of the sample completion times) is defined in terms of the ancilla optimization variables z_j for $j \in \{1, \dots, N\}$, that are bounded below by the arrival time of sample j at the rack after the schedule has finished.

3 Benchmark Setup

In the present section, we describe the design of the benchmark. We start with an outline of the considered problem instances that are listed in more detail in Appendix B. Subsequently, we describe the three different commercial technologies that we use.

3.1 Instances

To set the stage for our benchmark, we specify 260 test instances of our optimization problem of interest, each defined by a different set of parameters. Specifically, each instance is uniquely determined by the number of samples N , the number of photos K , the gaps $g_{j,k}$ between subsequent photos k and $k+1$ for

$k \in \{1, \dots, K-1\}$ and $j \in \{1, \dots, N\}$, and, finally, the processing times $p_{j,1}, p_{j,2}, p_{j,3}$ of the water mixer, sample shaker and photo booth, respectively, as explained in Section 2.2. For the sake of simplicity, the processing time of the photo booth agrees for all samples of the same instance, that is $p_{j,3} := p_3$ for all $j \in \{1, \dots, N\}$.

In Appendix B, we describe the algorithm that was used to generate parameter sets for the benchmark instances. Since the resulting instances span a wide range of complexity, we divide the resulting benchmark library into two parts, where each part is defined by the number of binary variables in the corresponding QUBO formulation from Section 2.2.2 as explained in Appendix A.1 in more detail. The first part, which we call *library of minor instances*, contains all 161 instances that have at least 2071 and at most 8080 binary variables. The second part, which we call *library of major instances*, contains the remaining 99 instances with at least 10 822 and at most 22 692 binary variables. The reason for that specific division is that 8192 is the maximal amount of variables that can be solved directly on Fujitsu’s digital annealer.

We collect groups of instances (N, K) that have the same number of samples and photos as shown in the boxplots in Fig. 4, i.e., within those groups the leftover parameters $p_{j,m}$ and $g_{j,k}$ for $j \in \{1, \dots, N\}, m \in \{1, 2, 3\}$ and $k \in \{1, \dots, K-1\}$ may vary. These groups can be understood as a collection of similar TRSPs. This approach allows us to consider statistical metrics over several instances when we compare models and solvers. In Appendix B, we list how many instances each group contains.

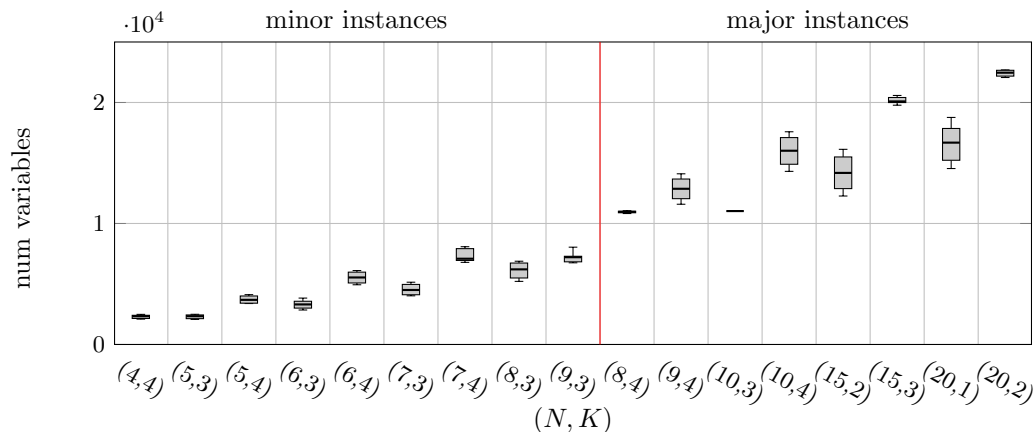


Figure 4: The number of variables of each group (N, K) of instances. The minor instances are left to the red vertical line, the major instances to the right.

3.2 Quantum and classical solvers

In our benchmark, we solve the generated instances with a selection of model and solver combinations with the main goal to assess the performance of quantum and quantum-inspired technology. Specifically, we consider three solver candidates:

1. Gurobi: As a baseline, we use the branch and bound algorithm of Gurobi, which is a state-of-the-art mathematical programming solver running on classical hardware (Gurobi Optimization, LLC 2023). In summary, it relies on an implicit enumeration that allows the original problem to be split into smaller sub-problems using a decision tree. The use of lower bounds derived from linear programming (LP) relaxations allows for a reduction of the search space. In this work we utilized the cloud based service of Gurobi solver, which ran on a Intel(R) Xeon(R) Platinum 8275CL CPU (3.00 GHz with 8 physical cores).

2. D-Wave’s hybrid *Leap* framework (LBQM): D-Wave provides cloud-based access to their adiabatic quantum computers with over 5000 qubits (D-Wave Systems Inc. 2020). By design, their hardware is specifically tailored to solve QUBOs. To this end, the QUBO is encoded in an Hamiltonian such that each optimization variable is represented by one qubit (Zbinden *et al.* 2020) and the ground state corresponds to the optimal solution. The quantum annealing mechanism aims to find the ground state by performing a suitable time evolution of the quantum system with a subsequent measurement of all qubits to reveal the optimal solution.

The D-Wave hardware has only limited connectivity, which means that each qubit can only interact with a certain number of other qubits. This limitation restricts the correlations between optimization variables that can be represented by the Hamiltonian. Finding a suitable representation with these constraints is an NP-hard problem (Lobe, Lutz 2022) that has to be solved classically to configure the quantum annealer for a certain problem. In practice, the quantum annealer can typically only be used for QUBOs with much less than 5000 optimization variables.

For this reason, D-Wave also provides a hybrid software framework LBQM, which is a black-box algorithm for binary quadratic models (BQMs) that runs on both classical and quantum annealing hardware. It allows to handle larger optimization problems that are too big for the quantum hardware by presenting only parts of the original problem to the quantum annealer. However, the exact mode of operation of LBQM is not publicly available. In this study, we use only the quantum annealer in a hybrid fashion via LBQM. The quantum machine used in the hybrid framework is the *D-Wave Advantage System 4.1* and the region *na-west-1*. We choose to use a constant number of 1000 samples (or readouts) for all evaluations and use default settings for all parameters.

3. Fujitsu’s digital annealer (FDA) and Fujitsu’s digital annealer hybrid framework (FDAh): The digital annealer from Fujitsu can be considered as a quantum-inspired algorithm that runs on dedicated (classical) hardware (Aramon *et al.* 2019) and can be accessed using a cloud service. It is based on simulated annealing (Kirkpatrick, Gelatt, Vecchi 1983; Černý 1985) with two major differences. Firstly, the utilization of an efficient parallel-trial scheme to exploit the parallelization capabilities of the hardware and, secondly, a dynamic escape mechanism to avoid locally optimal solutions. The detailed hardware specifications are confidential. The solver supports QUBOs with up to 8192 variables.

In addition, the hybrid solver FDAh is provided to solve bigger problem instances by utilizing both dedicated and classical hardware (Nakayama *et al.* 2021) similar to D-Wave’s LBQM. In this study, we use both FDA and FDAh. Both solvers require a set of parameters that specify how the annealing is done, which also include the number of repetitions and parallel runs on the chip. The specific parameters we used for FDA and FDAh are provided in Appendix C.

In a small pre-study, we excluded a few other solvers; see Appendix D.

Each instance can be modelled with each of the three modeling approaches from Section 2. However, not all solvers are applicable to all problem formulations and all instances. The MIP sequence model is solved with Gurobi for all instances. The time-indexed model is solved with Gurobi only for the minor instances. The QUBO model is solved with LBQM and FDA for minor instances. For major instances, the QUBO model is only solved with FDAh.

We call each valid model and solver combination an *approach* and use a unique name to refer to it. Summarized, we consider Gurobi with the sequence model (SE-GU), Gurobi with the time-indexed model (TI-GU), LBQM with the QUBO model (QU-LBQM), FDA with the QUBO model (QU-FDA) and FDAh with the QUBO model (QU-FDAh). An overview over all approaches is shown in Fig. 5.

For all problems, we prescribe a runtime limit of 3600 seconds for Gurobi. Both LBQM and FDA also require a time limit for each run, which scales with the problem size in the QUBO formulation as follows. The time limit for LBQM is set to be $\min\{100, 1.5 \cdot \frac{n}{100}\}$ seconds, where n is the number of variables in the QUBO formulation for the minor instances. The runtime of the digital annealer is implicitly set with the *steps* parameter, where each step taken in the annealing process takes a constant amount of time. We set the number of steps to be 10^7 for the instances with $2071 \leq n \leq 4096$, $5 \cdot 10^7$ for the ones with $4096 < n \leq 6000$ and 10^8 for the instances with $6000 < n \leq 8080$ variables in the

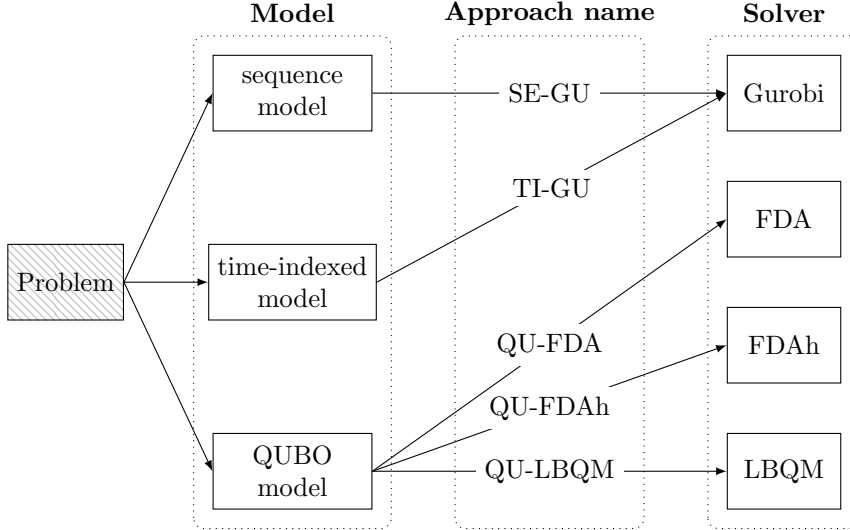


Figure 5: Summary of model (see Section 2.2) and solver (see Section 3.2) combinations for the benchmarks.

QUBO formulation. Lastly the major instances computed with the hybrid framework FDAh based on the digital annealer require a time limit as well. For this we distributed the available time of 5 hours to the instances, correspondingly to their number of variables. This computes approximately as $n \cdot 0.0117$ seconds where n is the number of variables in the QUBO formulation.

The benchmark setup is summarized in Table 1, where we recall the approaches from Fig. 5. The table also contains the values of the QUBO parameters ρ_0, \dots, ρ_7 from equation (23) that were chosen for LBQM, FDA and FDAh, respectively. The choice was made according to previous experiments with smaller problem instances. For this purpose, a typical strategy is to iteratively increase the parameter ρ_i if the corresponding penalty term P_i is non-vanishing. Additionally, one needs to make sure that the parameter ρ_0 for the target function is set such that it is not in favor to violate penalty terms and a good optimization is achieved.

4 Benchmark Results

In the current section, we present the results of our previously described benchmark, which is summarized in Table 1. For this purpose, we first show the results for the minor instances and subsequently the results for the major instances.

4.1 Results for Minor Instances

In Fig. 6, we show the objective values and runtimes of several approaches as boxplots. All runtimes are end-to-end runtimes, that is, we consider the entire evaluation pipeline, beginning with the submission of the problem to the solver and ending with the return of a solution, including potential network delays. The programmatic construction of the optimization problem for the application programming interface (API) of the solver based on the instance data is not part of the runtime.

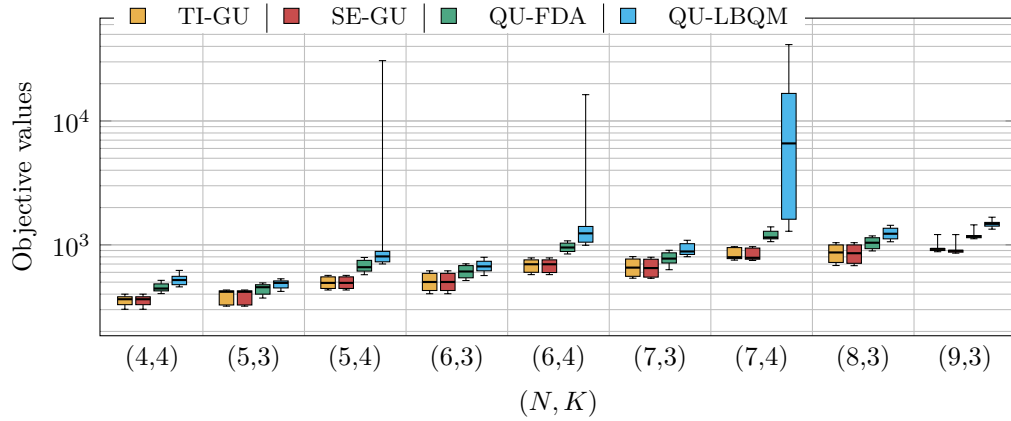
From Fig. 6a, we can observe that both the SE-GU and TI-GU solutions reach a better objective value than the solutions from QU-LBQM and QU-FDA. When comparing objective values, it has to be taken into account that the QUBO model objective, equation (2), also includes penalty terms, which become positive for infeasible solutions and therefore increase the objective value accordingly. Specifically, we

Table 1: Benchmark setup: Summary of problem instances from Section 3.1 and solvers from Section 3.2 for the optimization problems (or models) from Section 2.

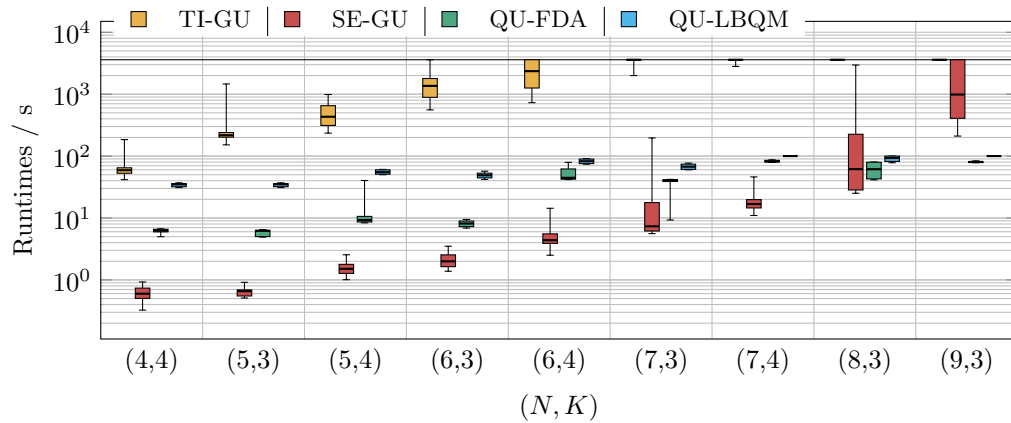
Property	Minor instances	Major instances
Number of instances	161	99
Number of variables (n)	2071 to 8080	10 822 to 22 692
Approach (cf. Fig. 5)	Used for minor instances	Used for major instances
SE-GU	✓	✓
TI-GU	✓	✗
QU-LBQM	✓	✗
QU-FDA	✓	✗
QU-FDAh	✗	✓
Approach (cf. Fig. 5)	Minor instance limit	Major instance limit
SE-GU	3600 s	3600 s
TI-GU	3600 s	—
QU-LBQM	$\min\{100, 1.5 \cdot \frac{n}{100}\} \cdot 1 \text{ s}$	—
QU-FDA	$1 \cdot 10^7$ iterations, $2071 \leq n \leq 4096$	—
	$5 \cdot 10^7$ iterations, $4096 < n \leq 6000$	
	$1 \cdot 10^8$ iterations, $6000 < n \leq 8080$	
QU-FDAh	—	$n \cdot 0.0117 \text{ s}$
Solver	QUBO parameters from equation (23)	
LBQM	$\rho_0 = 1, \rho_1 = 30\,000, \rho_2 = \rho_3 = \rho_4 = \rho_5 = \rho_7 = 10\,000, \rho_6 = 15\,000$	
FDA	$\rho_0 = 1000, \rho_1 = 4000, \rho_2 = \rho_3 = 1000, \rho_4 = \rho_5 = \rho_6 = \rho_7 = 1500$	
FDAh	$\rho_0 = 1000, \rho_1 = 2000, \rho_2 = \rho_3 = 500, \rho_4 = \rho_5 = \rho_6 = \rho_7 = 750$	

find that only QU-LBQM yields infeasible solutions for some instances, whereas all other approaches yield feasible solutions (SE-GU and TI-GU solutions are by definition always feasible). For our analysis, we include both feasible and infeasible solutions. By performing a Welch t-test (Welch 1947), we find that the means of the results from both SE-GU and TI-GU are lower than the means of the QU-FDA and QU-LBQM results with a statistical significance of over 99%, respectively. The same holds for the QU-FDA objective values in comparison to QU-LBQM.

On the other hand, according to Fig. 6b, the computation time for TI-GU and for some instances of SE-GU exceed the computation time of QU-LBQM and QU-FDA. Since MIP solvers typically spend a lot of time proving that a solution is optimal, we are also interested in the time taken by Gurobi (for both SE-GU and TI-GU) to find solutions of the same quality as those obtained from QU-LBQM or QU-FDA. Hence, we perform an additional analysis of the iterative solver progress of each Gurobi run and look for the earliest computation time at which Gurobi has reached an objective value that is less than or equal to the corresponding objective value returned by the competing solvers for the same instance. We call this earliest computation time the *relative runtime*. Specifically, we consider the relative runtime of TI-GU w.r.t. QU-LBQM (TI-GU@QU-LBQM), the relative runtime of SE-GU w.r.t. QU-LBQM (SE-GU@QU-LBQM), the relative runtime of TI-GU w.r.t. QU-FDA (TI-GU@QU-FDA) and the relative runtime of SE-GU w.r.t. QU-FDA (SE-GU@QU-FDA). In the special case that Gurobi is not able to find an objective value of the desired quality within its limit of 3600 seconds (which only occurs for some major instances), this time limit is used in place of the earliest computation time.



(a) Objective values



(b) Runtimes

Figure 6: Benchmark results for minor instances as boxplots. The results are grouped into sets of instances (N, K) with the same number of samples N and photos K . A horizontal line marks the upper time limit of 3600s for Gurobi in Fig. 6b. Some instances have not been solved to feasibility by QU-LBQM, as indicated by the peaks above 10^4 in Fig. 6a. Abbreviations according to Fig. 5.

Exemplarily, we consider a specific instance to visualize TI-GU@QU-LBQM and TI-GU@QU-FDA in Fig. 7.

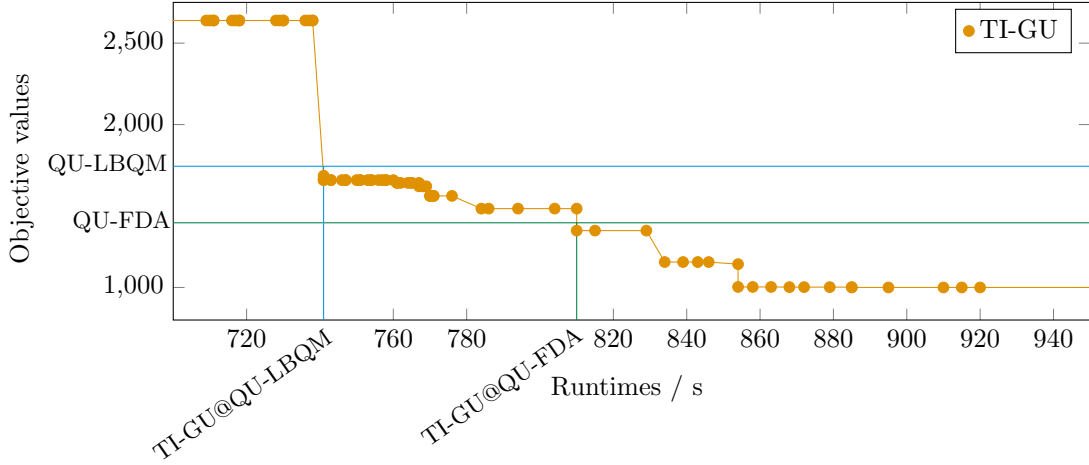


Figure 7: Visualization of the relative runtime of TI-GU w.r.t. QU-LBQM and QU-FDA, denoted by TI-GU@QU-LBQM and TI-GU@QU-FDA, respectively. Here, we consider the example instance $(7, 4, 3)(3)$; see supplementary material. The orange dots (connected by lines for better visualization) mark the resulting objective values of TI-GU at the corresponding time steps. The horizontal upper, blue and lower, green line mark the final objective value of QU-FDA and QU-LBQM, respectively, on the same instance. The blue and green lines intersect with the orange lines at some point. The time coordinate of the next lower TI-GU objective value after this intersection represents the relative runtime of TI-GU w.r.t. the solver, which is marked as a vertical line in the corresponding color. In other words, the relative runtime represents how long TI-GU has to run until it reaches an objective value that is at least as good as the result from QU-LBQM or QU-FDA, respectively.

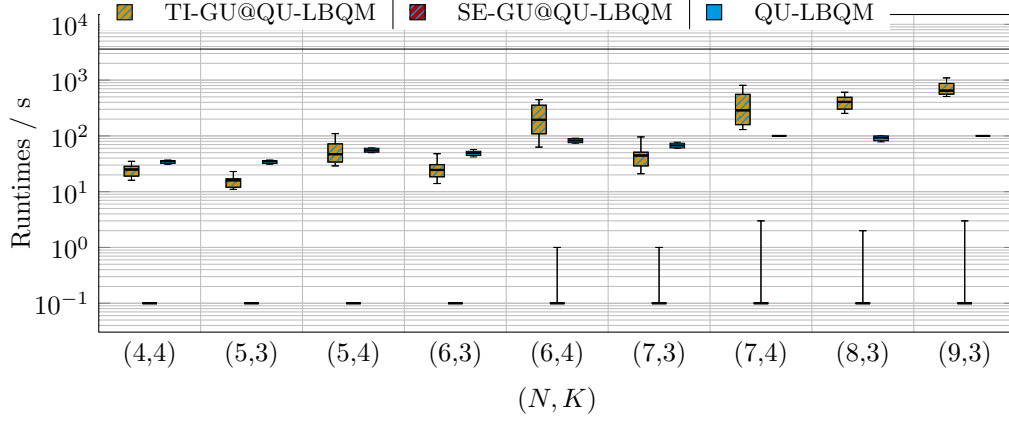
The results of this analysis are shown in Fig. 8. This plot shows that QU-LBQM is not able to compete with SE-GU. All problems from the first 4 out of 9 instance groups have been solved with SE-GU in under 1 second while the remaining instances in less than 10 seconds, whereas the QU-LBQM runtimes range between 50 and 100 seconds. However, LBQM finds a comparable solution faster than TI-GU for most problems with 6 or more samples and remains competitive for smaller problems. A Welch-t test confirms that the mean of TI-GU runtime is larger than the one of QU-LBQM runtime with a significance over 99%.

Furthermore, Fig. 8b shows that QU-FDA is outperformed by SE-GU as well. Analogous to Fig. 8a, the instances in groups $(4, 4)$, $(5, 3)$, $(5, 4)$ and $(6, 3)$ have been solved by SE-GU in 1 second or less. But in contrast to Fig. 8a, the other groups have their median between 1 second and 10 seconds, i. e., which reflects that the target objectives from QU-FDA are lower than those from QU-LBQM (see Fig. 6a). Nonetheless, the time taken for SE-GU to reach the solution quality of QU-FDA is 10 to 100 times smaller. Regarding TI-GU, QU-FDA finds a comparable solution almost always faster with a few exceptions.

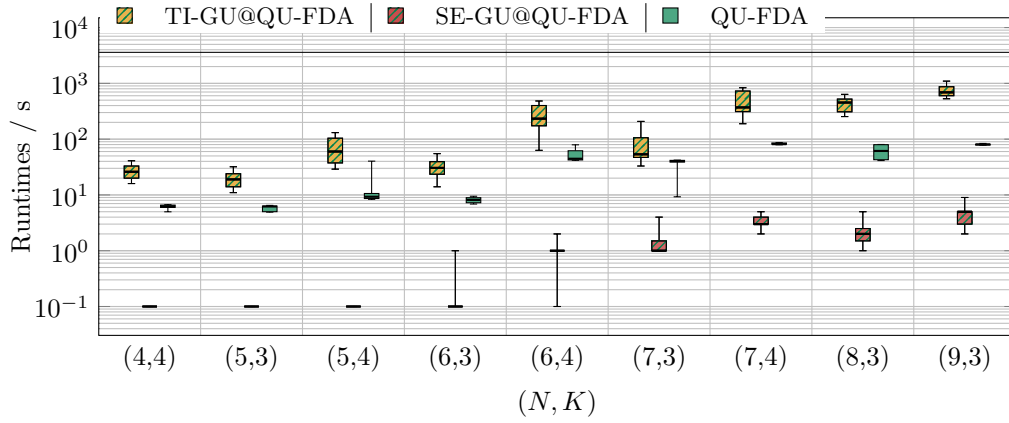
4.2 Results for Major Instances

The results for major instances are presented in analogy to the results for minor instances from the previous section. In Fig. 9, we show the runtime and the target value of the solvers on the corresponding models as boxplots.

The objective values of QU-FDAh are worse than the ones of SE-GU with a significance of over 97%, but Fig. 9a shows that the runtime of SE-GU increases strictly until it reaches the upper bound

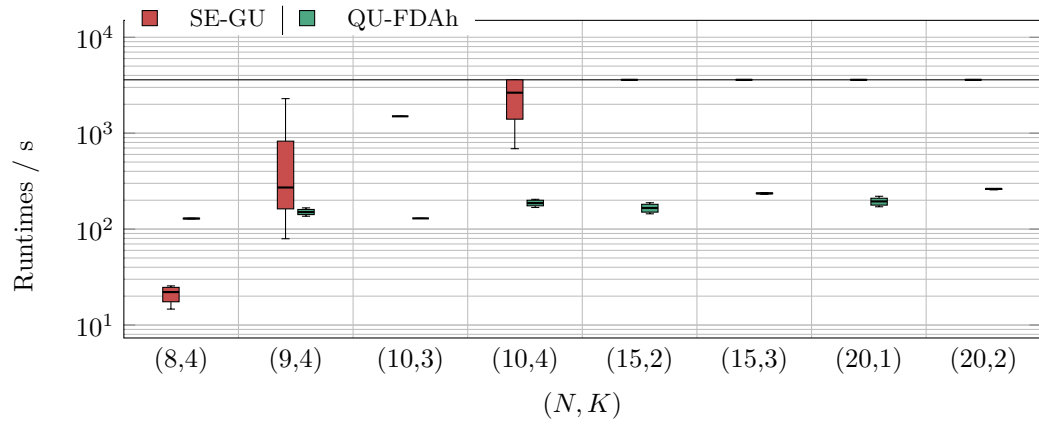


(a) Runtime comparison for TI-GU@QU-LBQM, SE-GU@QU-LBQM and QU-LBQM from Fig. 6b.

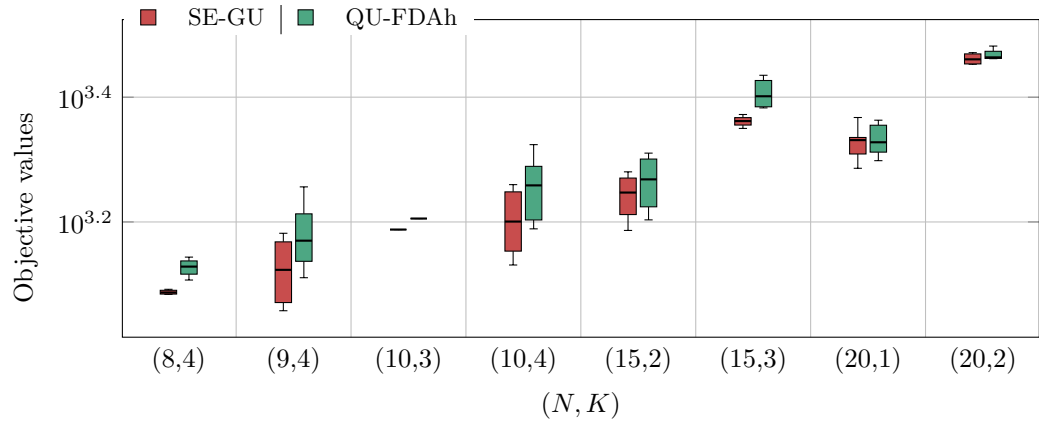


(b) Runtime comparison for TI-GU@QU-FDA, SE-GU@QU-FDA and QU-FDA from Fig. 6b.

Figure 8: Benchmark results for minor instances as boxplots. We show the relative runtimes of TI-GU and SE-GU w.r.t. QU-LBQM and QU-FDA, denoted by TI-GU@QU-LBQM, TI-GU@QU-FDA, SE-GU@QU-LBQM and SE-GU@QU-FDA, respectively. The results are grouped into sets of instances (N, K) in analogy to Fig. 6. See Fig. 7 for an example of the relative runtime computation. Abbreviations according to Fig. 5.



(a) Runtimes



(b) Objective values

Figure 9: Benchmark results for major instances as boxplots. The results are grouped into sets of instances (N, K) as for previous plots. Abbreviations according to Fig. 5.

for the computation time of 3600 seconds, which happens for ca. 15 samples. On the other hand, the computation time of QU-FDAh ranges between 120 and 300 seconds, where only a slight increase can be seen.

Analogously to Fig. 8b, we evaluate the earliest computation times of SE-GU model to reach objective values equal to or lower than the objective values obtained from QU-FDAh, denoted by the relative runtime of SE-GU w.r.t. QU-FDAh (SE-GU@QU-FDAh). The results are shown in Fig. 10.

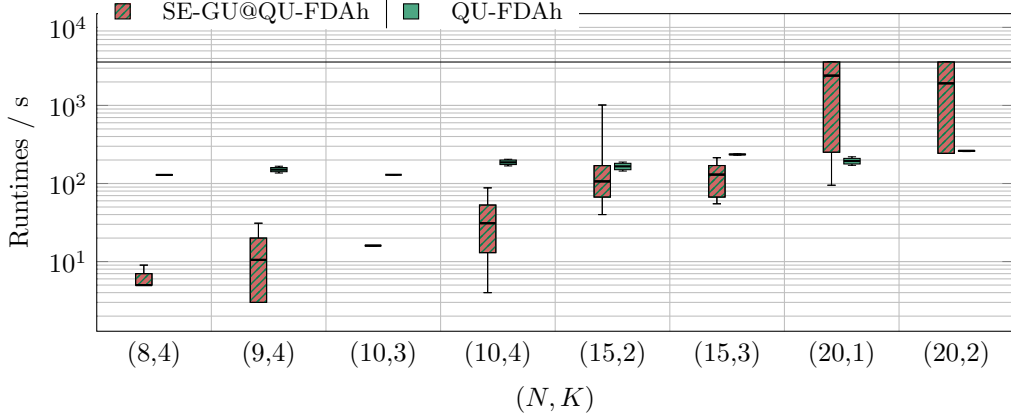


Figure 10: Benchmark results for major instances as boxplots. We show the relative runtime of SE-GU w.r.t. QU-FDAh, denoted by SE-GU@QU-FDAh, in analogy to Fig. 8. We also show the runtime of QU-FDAh from Fig. 9a. The results are grouped into sets of instances (N, K) as for previous plots. Abbreviations according to Fig. 5.

In Fig. 10, a strictly increasing computation time can be seen for SE-GU, whereas the QU-FDAh runtime remains almost constant. For the biggest instances with $N = 20$ samples, QU-FDAh has a clear advantage with respect to the computation time, whereas it is competitive to SE-GU for the instances with 15 samples. In this sense QU-FDAh finds a solution of comparable quality much faster for problems with 20 samples than SE-GU and the latter was not able to prove optimality for some of the instances with 20 samples. A Welch t-test confirms with a significance of over 99% that the QU-FDAh mean is lower than the SE-GU@QU-FDAh mean.

5 Conclusion and Outlook

This paper presents a thorough benchmarking of an industrially relevant use case of combinatorial optimization, the *transport robot scheduling problem* (TRSP) with the goal to achieve a time-optimal robot schedule, as motivated by a BASF high-throughput laboratory, see Fig. 1. We solve a large set of instances for this optimization problem with varying difficulty using three commercially available solvers: (i) the D-Wave quantum annealer, (ii) the quantum-inspired Fujitsu digital annealer and (iii) the classical state-of-the-art solver Gurobi. To this end, we develop several mathematical models: a quadratic unconstrained binary optimization (QUBO) model for the quantum and digital annealer and two different mixed integer program (MIP) models for Gurobi, which we call time-indexed and sequence model, respectively. Modeling the same problem in different, solver-specific forms helps us to optimally assess the capabilities of each solver. In total, we compare five different approaches (i. e., model and solver combinations as sketched in Fig. 5): (i) Gurobi with the time-indexed model (TI-GU), (ii) Gurobi with the sequence model (SE-GU), (iii) D-Wave’s hybrid *Leap* framework (LBQM) with the QUBO model (QU-LBQM), (iv) Fujitsu’s digital annealer (FDA) with the QUBO model (QU-FDA) and (v) Fujitsu’s digital annealer hybrid framework (FDAh) with the QUBO model (QU-FDAh). For our performance study, we separated all problem instances into two groups. First, the *minor instances* with problems less

than 10 000 binary variables in the QUBO formulation and, second, the *major instances* with problems with more than 10 000 and up to 22 000 variables. For practical reasons, we only solve the minor instances with SE-GU, TI-GU, QU-LBQM and QU-FDA, whereas the major instances are only solved with SE-GU and QU-FDAh, respectively.

Our benchmark reveals insights both regarding the objective values of the optimization problem (i. e., the sum of sample completion times) as well as the end-to-end runtimes for the considered approaches. Regarding the objective values, we observe for minor instances that SE-GU and TI-GU give similar results, outperforming QU-FDA, which in turn outperforms QU-LBQM (cf. Fig. 6a). For major instances, SE-GU outperforms QU-FDAh (cf. Fig. 9b). Regarding the runtime, we find that for smaller instances TI-GU takes the highest time and SE-GU takes mostly the lowest. Between these two extremes, QU-FDA and QU-LBQM take about the same amount of time (cf. Fig. 6b). However, the runtime of SE-GU significantly increases with increasing instance complexity. This same observation continues for the large instances, for which the runtime of SE-GU is mostly larger than that of QU-FDAh (cf. Fig. 9a).

To get further insights into the relationship between objective value and runtime, we also studied the relative runtime of Gurobi, that is the time that Gurobi took to find an objective value that is at least as good as the final result from another approach. For minor instances, we find that the relative runtimes of SE-GU w.r.t. QU-LBQM and QU-FDA, respectively, are strictly lower than the runtimes of QU-LBQM and QU-FDA, i. e., Gurobi found solutions of comparable quality faster than the quantum and quantum-inspired approaches (cf. Figs. 8a and 8b). This is not surprising since SE-GU tended to find better objectives in shorter time. For major instances, the relative runtimes of SE-GU w.r.t. QU-FDAh increase significantly with increasing instance complexity and clearly exceed the runtime of QU-FDAh for the biggest instances (cf. Fig. 10). Thus, QU-FDAh shows an advantage on some bigger instances. Although the resulting objective values of QU-FDAh were not optimal, the approach shows a clear advantage on some bigger instances when compared to SE-GU on a similar time scale.

Summarized, no general advantage of the quantum and quantum-inspired solvers was found. However, for certain instances the quantum-inspired hybrid usage of the Fujitsu digital annealer turned out to be a very promising alternative to Gurobi and was clearly superior to a hybrid usage of D-Wave’s quantum annealer. Our study is not a conclusive result but rather an application-oriented case study that provides a snapshot of the current technology and leaves room for performance improvements on the modeling as well as the solver side. For example, an improvement of the quantum annealer might be possible with additional problem-specific fine-tuning of the annealing schedule or other hardware-related parameters. Moreover, the recently released constrained quadratic model (CQM) solver from D-Wave also promises to provide much better performance compared to the solver used in this work. Especially in an agile field such as quantum computing, a technology snapshot such as ours can hardly provide any forecasts about future developments. Therefore, in order to preserve an up-to-date assessment, further practical evaluations for real-world use cases will be necessary. The methods and results from this project can serve as a blueprint or at least point of reference for this kind of ongoing research.

6 Acknowledgements

We would like to thank Behrang Shafei, Jens Meissner and Horst Weiss for their invaluable input and support throughout the research process. Without their ongoing contributions, the work would not have been accomplished.

A Models

All models shown in this section use the following problem parameters:

- machines: M_1 (water mixer), M_2 (sample shaker), M_3 (photo booth),
- samples: $j \in \{1, 2, 3, \dots, N\}$,
- machine processing times: $p_{j,m}$ for $j \in \{1, \dots, N\}$, $m \in \{1, 2, 3\}$,
- time (slots): $t \in \{0, \dots, T - 1\}$,

- photos: $k \in \{1, \dots, K\}$,
- gap between photos k and $k + 1$ of sample $j \in \{1, \dots, N\}$: $g_{j,k}$ for $k \in \{1, \dots, K - 1\}$.

A.1 QUBO Model

A.1.1 Variables

The QUBO model uses the variables

$$x_{j,m,t} := \begin{cases} 1, & \text{if sample } j \text{ starts processing on machine } M_m \text{ at time } t, \\ 0, & \text{otherwise} \end{cases} \quad (8)$$

with $x_{j,m,t} \in \{0, 1\}$ for all $j \in \{1, \dots, N\}$, $m \in \{1, 2, 3\}$ and $t \in \{1, \dots, T - 1\}$. Here,

$$T := T(N, K, p, g) := \left(\sum_{j=1}^N p_{j,1} + p_{j,2} + K \cdot p_{j,3} \right) + \left(\sum_{j=1}^N \sum_{k=1}^{K-1} g_{j,k} \right) + N \cdot (3 + K) \quad (9)$$

is the time horizon for an instance with parameters $N, K, p := \{p_{j,m} \mid j \in \{1, \dots, N\}, m \in \{1, 2, 3\}\}$, $g := \{g_{j,k} \mid j \in \{1, \dots, N\}, k \in \{1, \dots, K - 1\}\}$.

In total, there are $N \cdot 3 \cdot T(N, K, p, g)$ binary variables. However, a certain subset of these variables can by definition be fixed to 0 to reduce the number of effective optimization variables:

- i) The processing of any job on machines M_1, M_2 and M_3 can only start after the preceding processes are finished. Thus, for all $j \in \{1, \dots, N\}$ and $m \in \{1, 2, 3\}$ we set

$$x_{j,m,t} = 0 \quad \forall t : 0 \leq t \leq m - 1 + \sum_{m'=1}^{m-1} p_{j,m'}. \quad (10)$$

- ii) Analogously the latest start for a process on machines M_1 and M_2 can be bounded by $T - 1$ minus the total time taken by the subsequent processes. For all jobs $j = 1, \dots, N$ and $m = 1, 2$ we set

$$x_{j,m,t} = 0 \quad \forall t : (T - 1) - \left(\sum_{k=1}^{K-1} g_{j,k} + K \cdot p_{j,3} + \sum_{m'=m}^2 (1 + p_{j,m'}) \right) \leq t \leq T - 1. \quad (11)$$

Summarized, $c(N, K, p, g)$ variables are required to attain a constant value of zero to achieve feasibility with $c(N, K, p, g)$ being the number of variables set to zero according to equations (10) and (11). Consequently, we arrive at a QUBO with

$$n := N \cdot 3 \cdot T(N, K, p, g) - c(N, K, p, g) \quad (12)$$

binary optimization variables $x_{j,m,t}$.

A.1.2 Constraints

In the following, we write x for the vector consisting of these n optimization variables in an arbitrary but fixed order.

With this notation, the penalty terms for the QUBO read:

- 1) Each sample is processed precisely once by M_1 and M_2 .

$$P_1(x) := \sum_{j=1}^N \sum_{m=1}^2 \left[\left(\sum_{t=1}^{T-1} x_{j,m,t} \right) - 1 \right]^2. \quad (13)$$

- 2) All samples are processed K times by the photo booth M_3 .

$$P_2(x) := \sum_{j=1}^N \left[\left(\sum_{t=1}^{T-1} x_{j,3,t} \right) - K \right]^2. \quad (14)$$

- 3) No two processings can start at the same time (because processings start immediately when a sample is brought to a machine).

$$P_3(x) := \sum_{t=0}^{T-1} \left(\sum_{j=1}^N \sum_{m=1}^3 x_{j,m,t} \right) \left[\left(\sum_{j=1}^N \sum_{m=1}^3 x_{j,m,t} \right) - 1 \right]. \quad (15)$$

- 4) A machine M_m is occupied in the time frame between t and $t + p_{j,m}$ in the case that any sample j has been put on it at time t .

$$P_4(x) := \sum_{m=1}^3 \sum_{j=1}^N \sum_{t=0}^{T-1} \left(x_{j,m,t} \cdot \sum_{j' \neq j=1}^N \sum_{t'=t+1}^{\min\{t+p_{j,m}, T-1\}} x_{j',m,t'} \right) \quad (16)$$

- 5) Processing of a sample on consecutive machines must not overlap.

$$P_5(x) := \sum_{m=1}^2 \sum_{j=1}^N \sum_{t=0}^{T-1} \left(x_{j,m+1,t} \cdot \sum_{t'=\max\{t-p_{j,m}, 0\}}^{T-1} x_{j,m,t'} \right) \quad (17)$$

- 6) After a sample is processed at machine M_2 , it needs to be immediately brought to the photo booth, and the subsequent photos need to be taken at specific times later.

Let $\gamma_{j,k} := 1 + \sum_{k'=1}^{k-1} g_{j,k'} + p_{j,3} \cdot (k-1)$ for $k \in \{1, \dots, K\}$ be the desired gap between the end of the shaking process on M_2 and start of the k th photo on M_3 . Set

$$P_6(x) := \sum_{j=1}^N \sum_{k=1}^K \sum_{t=0}^{T-1-\gamma_{j,K}} x_{j,2,t} \cdot (1 - x_{j,3,t+\gamma_{j,k}+p_{j,2}}). \quad (18)$$

- 7) Certain pairs of tasks require a gap of one time unit between them for the robot to travel between the machines and the rack empty-handed. We set $P_7 := P_{7.1} + P_{7.2} + P_{7.3}$ where $P_{7.1}$, $P_{7.2}$ and $P_{7.3}$ are defined as follows:

- 7.1) If a job j is put on a machine M_m at time t , then no job can be put on any machine at time $t + 1$.

$$P_{7.1}(x) := \sum_{t=0}^{T-2} \left(\sum_{j=1}^N \sum_{m=1}^3 x_{j,m,t} \cdot \sum_{j'=1}^N \sum_{m'=1}^3 x_{j',m',t+1} \right) \quad (19)$$

- 7.2) If a job j is picked up from a machine M_m at time t , then no other job j' can be picked up from any other machine at times t and $t + 1$.

$$P_{7.2}(x) := \sum_{t=0}^{T-2} \sum_{j=1}^N \left(\sum_{m=1}^3 x_{j,m,t-p_{j,m}} \cdot \sum_{j'=1}^N \sum_{\substack{m'=1 \\ m' \neq m}}^3 (x_{j',m',t-p_{j',m'}} + x_{j',m',t+1-p_{j',m'}}) \right) \quad (20)$$

- 7.3) If a job j is picked up from a machine M_m at time t , then no other job can be put on any machine at times t and $t + 1$.

$$P_{7.3}(x) := \sum_{t=0}^{T-1} \sum_{m=1}^3 \left(\sum_{j=1}^N x_{j,m,t-p_{j,m}} \cdot \sum_{\substack{j'=1 \\ j' \neq j}}^N \sum_{m'=1}^3 (x_{j',m',t} + x_{j',m',t+1}) \right) \quad (21)$$

A.1.3 Objective

The objective function computes as

$$F(x) := \sum_{j=1}^N \sum_{t=1}^{T-1} \left(t + p_{j,2} + 1 + K \cdot p_{j,3} + \sum_{k=1}^{K-1} g_{j,k} + 1 \right) \cdot x_{j,2,t}. \quad (22)$$

A.1.4 Summary

Altogether, the *QUBO model* is defined as:

$$\begin{aligned} \min_x \quad & \rho_0 F(x) + \sum_{i=1}^7 \rho_i P_i(x) \\ \text{s.t.} \quad & x \in \{0, 1\}^n \end{aligned} \quad (23)$$

A.2 Sequence Model

A.2.1 Variables

We define the event set $E := \{(j, i, a) \mid j \in \{1, \dots, N\}, i \in \{1, \dots, 2+K\}, a \in \{0 \text{ (place)}, 1 \text{ (pick up)}\}\}$, where event

$$(j, i, a) \text{ represents action } a \text{ for sample } j \begin{cases} \text{on machine } i & \text{for } i \leq 2; \\ \text{at the camera for photo } i-2 & \text{for } i \geq 3. \end{cases} \quad (24)$$

The following variables are used in the sequence model:

- $\tau_e \in \mathbb{R}_{\geq 0}$: Time of event e for all $e \in E$.
- $\delta_{m,j,j'} = \begin{cases} 1, & \text{if sample } j \text{ is processed by machine } m \text{ before sample } j', \\ 0, & \text{otherwise,} \end{cases}$
for all $m \in \{1, 2\}, j, j' \in \{1, \dots, N\}, j \neq j'$.
- $\varepsilon_{e,f} = \begin{cases} 1, & \text{if event } e \text{ happens before event } f, \\ 0, & \text{otherwise,} \end{cases}$
for all $e = (j, i, a), f = (j', i', a') \in E, j \neq j', i \neq i', \min\{i, i'\} \leq 2$.
- $\zeta_{k,j,k',j'} = \begin{cases} 1, & \text{if the } k\text{th photo of sample } j \text{ is taken before the } k'\text{th photo of sample } j', \\ 0, & \text{otherwise,} \end{cases}$
for all $j, j' \in \{1, \dots, N\}$, for all $k, k' \in \{1, \dots, K\}$ with $j \neq j', k \neq k'$.

A.2.2 Constraints

To formulate the constraints we introduce the following notation:

- For $j \in \{1, \dots, n\}$ and $k \in \{1, \dots, K\}$ we denote by $\gamma_{j,k} := 1 + \sum_{k'=1}^{k-1} g_{j,k'} + (k-1) \cdot p_{j,3}$ the gap between the end of the shaking process of sample j and the beginning of the process of the k th photo.
- $\Gamma := \sum_{j=1}^N \left[\left(\sum_{m=1}^3 p_{j,i} + 1 \right) + \gamma_{j,K} + 1 \right]$ is a sufficiently large constant that is used for the ‘‘Big M’’ method (Griva, Nash, Sofer 2009).

Then we define the following list of constraints:

- 1) No two samples are processed on neither the water mixer nor the sample shaker at the same time.

$$\delta_{m,j,j'} + \delta_{m,j',j} = 1 \quad \forall m \in \{1, 2\}, j, j' \in \{1, \dots, N\}, j \neq j'. \quad (C_1)$$

- 2) The robot cannot perform two events of different samples at different places at the same time.

$$\varepsilon_{e,f} + \varepsilon_{f,e} = 1 \quad \forall e = (j, i, a), f = (j', i', a') \in E, j \neq j', i \neq i'. \quad (C_2)$$

- 3) No two samples can be at the photo booth for different photos at the same time.

$$\zeta_{k,j,k',j'} + \zeta_{k',j',k,j} = 1 \quad \forall j, j' \in \{1, \dots, N\}, k, k' \in \{1, \dots, K\}, j \neq j', k \neq k'. \quad (C_3)$$

4) The sample must be picked up exactly after its processing time.

$$\tau_{(j,i,1)} = \tau_{(j,i,0)} + p_{j,i} \quad \forall j \in \{1, \dots, N\}, i \in \{1, 2\}. \quad (C_4)$$

5) The transportation time of 1 time unit must be waited for.

$$\tau_{(j,i',0)} \geq \tau_{(j,i,1)} + 1 \quad \forall j \in \{1, \dots, N\}, i, i' \in \{1, \dots, 2 + K\}, i' > i. \quad (C_5)$$

6) The time frames at water mixer and sample shaker must match the orders specified by the δ -variables. The robot must first bring a sample away and can then get another one.

$$\tau_{(j',i,0)} \geq \tau_{(j,i,1)} + 2 - \Gamma \cdot \delta_{i,j',j} \quad \forall i \in \{1, 2\}, j, j' \in \{1, \dots, N\}, j \neq j'. \quad (C_6)$$

7) The k th photos of different samples must not overlap.

$$\tau_{(j',2+k,0)} \geq \tau_{(j,2+k,1)} + 2 - \Gamma \cdot \delta_{2,j',j} \quad \forall j, j' \in \{1, \dots, N\}, j \neq j', k \in \{1, \dots, K\}. \quad (C_7)$$

8) Different photos of different samples must not overlap.

$$\tau_{(j',2+k',0)} \geq \tau_{(j,2+k,1)} + 2 - \Gamma \cdot \zeta_{k',j',k,j} \quad \forall j, j' \in \{1, \dots, N\}, k, k' \in \{1, \dots, K\}, j \neq j', k \neq k'. \quad (C_8)$$

9) The times of the events of different samples at different machines must match the order and the robot must have enough time in between.

$$\tau_f \geq \tau_e - \Gamma \cdot \varepsilon_{f,e} + 2 \quad \forall e = (j, i, 1), f = (j', i', a') \in E, j \neq j', i \neq i', \min\{i, i'\} \leq 2. \quad (C_{9.1})$$

$$\tau_f \geq \tau_e - \Gamma \cdot \varepsilon_{f,e} + 2 \quad \forall e = (j, i, a), f = (j', i', 0) \in E, j \neq j', i \neq i', \min\{i, i'\} \leq 2. \quad (C_{9.2})$$

$$\tau_f \geq \tau_e - \Gamma \cdot \varepsilon_{f,e} + 1 \quad \forall e = (j, i, 0), f = (j', i', 1) \in E, j \neq j', i \neq i', \min\{i, i'\} \leq 2. \quad (C_{9.3})$$

10) The photo times must have the correct distance to the end of the shaking process.

$$\tau_{(j,2+k,0)} = \tau_{(j,2,1)} + \gamma_{j,k} \quad \forall j \in \{1, \dots, N\}, k \in \{1, \dots, K\}. \quad (C_{10.1})$$

$$\tau_{(j,2+k,1)} = \tau_{(j,2,1)} + \gamma_{j,k} + p_{j,3} \quad \forall j \in \{1, \dots, N\}, k \in \{1, \dots, K\}. \quad (C_{10.2})$$

A.2.3 Objective

The objective function computes as

$$F(\tau, \delta, \varepsilon, \zeta) := \sum_{j=1}^N (\tau_{(j,2+K,1)} + 2). \quad (25)$$

Note that by definition of the model, it is a valid solution that a sample is placed at time 0 on machine M_1 , which implies that the robot transports the sample at time -1 from the rack to M_1 . To overcome this we add an extra $+1$ to each sample to shift the whole schedule to the right. This does not affect the optimization process itself, but is rather a linear translation of the whole schedule w.r.t. the objective function to get a schedule starting at 0 in compliance with the other models. Lastly the sample arrives at the rack one time unit after the K 'th photo has been shot, thus we add another $+1$.

A.2.4 Summary

Altogether, the *sequence model* is defined as:

$$\begin{aligned} & \min_{\tau, \delta, \varepsilon, \zeta} F(\tau, \delta, \varepsilon, \zeta) \\ & \text{s.t. } C_1, \dots, C_8, C_{9.1}, C_{9.2}, C_{9.3}, C_{10.1}, C_{10.2} \\ & \tau_e \in \mathbb{R}_{\geq 0} \quad \forall e \in E \\ & \delta_{m,j,j'} \in \{0, 1\} \quad \forall m \in \{1, 2\}, j, j' \in \{1, \dots, N\}, j \neq j' \\ & \varepsilon_{e,f} \in \{0, 1\} \quad \forall e = (j, i, a), f = (j', i', a') \in E, j \neq j', i \neq i', \min\{i, i'\} \leq 2 \\ & \zeta_{k,j,k',j'} \in \{0, 1\} \quad \forall j, j' \in \{1, \dots, N\}, \forall k, k' \in \{1, \dots, K\} \text{ with } j \neq j', k \neq k' \end{aligned} \quad (26)$$

A.3 Time-Indexed Model

A.3.1 Variables

The time-indexed model makes use of the binary variables

$$y_{j,r,t} := \begin{cases} 1, & \text{if sample } j \text{ is transported by the robot on route } r \text{ at time } t, \\ 0, & \text{otherwise} \end{cases} \quad (27)$$

for all $j \in \{1, \dots, N\}$, $r \in \{1, \dots, 8\}$ and $t \in \{0, \dots, T-1\}$, where the routes r are given by Fig. 3. The time horizon T is defined as in equation (9). Additionally we have variables $z_j \in \mathbb{R}_{\geq 0}$ for $j \in \{1, \dots, N\}$ that are used to define the objective function (see equation (28)).

Setting M_0 to be the rack we define $r^-(i)$ to be the set of incoming routes and $r^+(i)$ the set of outgoing routes of M_i for $i \in \{0, 1, 2, 3\}$, i. e. $r^-(0) = \{2, 5, 8\}$, $r^+(0) = \{1, 4, 7\}$, $r^-(1) = \{1\}$ and so on. The set of all routes is $R := \{1, \dots, 8\}$.

A.3.2 Constraints

We define the following constraints:

- 1) The transport robot can carry at most one sample at a time.

$$\sum_{j=1}^N \sum_{r=1}^8 y_{j,r,t} \leq 1 \quad \forall t \in \{0, \dots, T-1\}. \quad (C_1)$$

- 2) The transport robot cannot teleport from one machine to another. For every time t and every machine i the robot cannot serve some route to i during $(t, t+1)$ and a route starting from another machine during $(t+1, t+2)$.

$$\sum_{j=1}^N \left[\left(\sum_{r \in r^-(i)} y_{j,r,t} \right) + \sum_{r \in R \setminus r^+(i)} y_{j,r,t+1} \right] \leq 1 \quad \forall i \in \{0, \dots, 3\}, t \in \{0, \dots, T-2\}. \quad (C_2)$$

- 3) Every machine may be occupied by at most one sample.

$$\sum_{j=1}^N \sum_{t'=0}^t \left[\left(\sum_{r \in r^-(i)} y_{j,r,t'} \right) - \sum_{r \in r^+(i)} y_{j,r,t'} \right] \leq 1 \quad \forall i \in \{1, 2, 3\}, t \in \{0, \dots, T-1\}. \quad (C_3)$$

- 4) Every sample is transported to the water mixer M_1 exactly once.

$$\sum_{t=0}^{T-1} y_{j,1,t} = 1 \quad \forall j \in \{1, \dots, N\}. \quad (C_4)$$

- 5) Samples can only be picked up from a machine, when they have been brought to it and stayed there for the appropriate time.

$$\sum_{t'=0}^t \sum_{r \in r^+(i)} y_{j,r,t'} = \sum_{t'=0}^{t-p_{i,j}-1} \sum_{r \in r^-(i)} y_{j,r,t'} \quad \forall j \in \{1, \dots, N\}, i \in \{1, 2, 3\}, t \in \{0, \dots, T-1\}. \quad (C_5)$$

- 6) Routes between rack and the first two machines must be driven along in the correct order.

$$\sum_{t'=0}^t y_{j,4,t'} \leq \sum_{t'=0}^{t-1} y_{j,2,t'} \quad \forall j \in \{1, \dots, N\}, t \in \{0, \dots, T-1\}. \quad (C_6)$$

- 7) At no time has a sample been brought from the rack to the camera more often than from the camera or the shaker to the rack.

$$\sum_{t'=0}^t y_{j,7,t'} \leq \sum_{t'=0}^{t-1} (y_{j,5,t'} + y_{j,8,t'}) \quad \forall j \in \{1, \dots, N\}, t \in \{0, \dots, T-1\}. \quad (C_7)$$

- 8) A sample is picked up from the camera at time t if and only if it has been placed there at time $t - p_{j,3}$, i. e., $y_{j,8,t} = 0$ for $t \leq p_{j,3}$ and $y_{j,8,t} = y_{j,6,t-p_{j,3}-1} + y_{j,7,t-p_{j,3}-1}$ for $t > p_{j,3}$. These constraints are equivalent to

$$\sum_{t'=0}^t y_{j,8,t'} = \sum_{t'=0}^{t-p_{j,3}-1} (y_{j,6,t'} + x_{j,7,t'}) \quad \forall j \in \{1, \dots, N\}, t \in \{0, \dots, T-1\}. \quad (C_8)$$

- 9) Every sample has to be picked up from the shaker early enough for the last photo.

$$\sum_{t=0}^{T-1-p_{j,3}-\gamma_{j,K}} (y_{j,5,t} + y_{j,6,t}) = 1 \quad \forall j \in \{1, \dots, N\}. \quad (C_9)$$

- 10) Every sample has to be picked up from the camera the same number of times as it is placed there.

$$\sum_{t=0}^{T-1} (y_{j,6,t} + y_{j,7,t} - y_{j,8,t}) = 0 \quad \forall j \in \{1, \dots, N\}. \quad (C_{10})$$

- 11) Samples must be at the camera at photo dates.

$$y_{j,5,t} + y_{j,6,t} \leq \sum_{t'=0}^{t+\gamma_{j,k}-1} (y_{j,6,t'} + y_{j,7,t'}) - \sum_{t'=0}^{t+\gamma_{j,k}+p_{j,3}-1} y_{j,8,t'} \quad \forall j \in \{1, \dots, N\}, \\ k \in \{1, \dots, K\}, t \in \{0, \dots, T - \gamma_{j,k} - p_{j,3}\}. \quad (C_{11})$$

- 12) Lastly we define a constraint that bounds the objective variables z_j below by the arrival time of sample j at the rack after the schedule has finished.

$$(t+1) \cdot y_{j,8,t} \leq z_j \quad \forall j \in \{1, \dots, N\}, t \in \{0, \dots, T-1\}, \quad (C_F)$$

A.3.3 Objective

Let y, z be vectors achieved by writing the corresponding variables into a vector in some arbitrary but fixed order. Using the constraint C_F , equation (C_F), the objective function simply computes as

$$F(y, z) := \sum_{j=1}^N z_j. \quad (28)$$

A.3.4 Summary

Altogether, the *time-indexed model* is defined as:

$$\begin{aligned} \min_{y,z} \quad & F(y, z) \\ \text{s.t.} \quad & C_1, \dots, C_{11}, C_F \\ & y_{j,r,t} \in \{0, 1\} \quad \forall j \in \{1, \dots, N\}, r \in \{1, \dots, 8\}, t \in \{0, \dots, T-1\} \\ & z_j \in \mathbb{R}_{\geq 0} \quad \forall j \in \{1, \dots, N\} \end{aligned} \quad (29)$$

B Benchmark Library

It is our goal to define a representative benchmark library with meaningful instances. For this purpose, we specify a set of relevant values for each parameter as listed in Table 2. We consider all 120 parameter combinations $N \in D_N$, $K \in D_K$ and $p_3 \in D_{p_3}$. For each combination, the remaining parameters are then drawn uniformly from the corresponding set of allowed values 10 times, which leads to 1200 instances in total.

Table 2: Parameter configurations for our benchmark instances.

Parameter	Choice	Domain
N	all	$D_N := \{1, 2, \dots, 10, 15, 20, 25, 50, 100\}$
K	all	$D_K := \{1, 2, 3, 4\}$
p_3	all	$D_{p_3} := \{1, 3\}$
$p_{j,1}$	random	$D_{p_1} := \{4, 5, 6, 7, 8\}$
$p_{j,2}$	random	$D_{p_2} := \{1, 2, 3, 4\}$
$g_{j,1}$	random	$D_{g_1} := \{4, 5\}$
$g_{j,2}$	random	$D_{g_2} := \{8, \dots, 12\}$
$g_{j,3}$	random	$D_{g_3} := \{16, \dots, 24\}$

However, we filter these instances such that only a relevant subset remains. Specifically, we only keep the instances with at least 2071 and at most 22 692 binary variables in the corresponding QUBO formulation from Section 2.2.2. This excludes the very easy and the very hard cases. A complete list with all computed instances, their parameters and the benchmark results is appended as supplementary information.

We collect groups of instances (N, K) that have the same number of samples N and photos K . In Table 3, we list how many instances each group contains.

C Fujitsu Solver Settings

Both FDA and FDAh have various parameters that can be used to tune the solver runs. Table 4 and Table 5 contain the values for each parameter of both solvers that was used in the benchmark.

D Pre-study

Before we started with the actual benchmarks for this paper, we performed a small pre-study in which we exemplarily tested our solver candidates on a few instances to assess their overall behavior. This allowed us to exclude three potential solver candidates beforehand. In this appendix section, we briefly summarize our qualitative observations for these excluded solvers:

- First, it turned out that quantum approximate optimization algorithm (QAOA) on the IBM gate-based quantum computers (IBM Quantum 2023) is very limited in problem size (up to $\sim 10^2$ variables) and, in addition, has an end-to-end runtime that is magnitudes longer than that of all other solvers due to the queuing system of the cloud service which can lead to major delays.
- Second, Quera’s Rydberg quantum computer *Aquila* (Wurtz *et al.* 2023) does not support local detuning, which is necessary for the QUBO encoding from Ref.(Nguyen *et al.* 2023), and we did not find an alternative MIP representation of our use case.
- Third, Toshiba’s Simulated Bifurcation Machine (TSB) had a very bad performance on all test instances and did not yield feasible solutions.

Sven: see my overleaf comment.

Table 3: Size informations about the instance groups: Number of instances as well as minimum and maximum number of variables for the the corresponding QUBO formulation.

(N, K)	Num. instances	Min num. vars	Max num. vars
(4, 4)	19	2096	2488
(5, 3)	15	2071	2494
(5, 4)	20	3384	4118
(6, 3)	20	2849	3834
(6, 4)	20	4935	6109
(7, 3)	20	4022	5146
(7, 4)	16	6787	8080
(8, 3)	20	5215	6880
(9, 3)	11	6750	8042
(8, 4)	4	10 822	11 058
(9, 4)	20	11 590	14 106
(10, 3)	1	11 026	11 026
(10, 4)	20	14 307	17 580
(15, 2)	20	12 270	16 129
(15, 3)	10	19 775	20 581
(20, 1)	20	14 541	18 765
(20, 2)	4	22 064	22 692

Table 4: FDA parameters. Here, k_{iter} denotes the number of iterations for QU-FDA as declared in the column “Minor instance limit” of Table 1.

Parameter	Value
“access_profile_file”	“AUTO”
“processor”	“DAv2”
“connection_mode”	“async”
“DAv2_optimization_method”	“annealing”
“DAv2_number_iterations”	k_{iter}
“DAv2_number_runs”	32
“DAv2_temperature_start”	10 000
“DAv2_temperature_end”	10
“DAv2_temperature_mode”	0
“DAv2_temperature_interval”	$k_{\text{iter}}/1\,000\,000$
“DAv2_offset_increase_rate”	100
“DAv2_solution_mode”	“COMPLETE”
“DAv2_bit_precision”	16

Table 5: FDAh parameters. Here, k_{time} denotes the time limit for QU-FDAh as declared in the column “Major instance limit” of Table 1.

Parameter	Value
“access_profile_file”	“AUTO”
“processor”	“DAv3”
“connection_mode”	“async”
“DAv3_time_limit_sec”	k_{time}
“DAv3__use__target_energy”	“False”
“DAv3_target_energy”	0
“DAv3_num_solution”	16
“DAv3_num_group”	4
“DAv3_num_output_solution”	5
“DAv3_gs_num_iteration_factor”	5
“DAv3_gs_num_iteration_cl”	200
“DAv3_gs_penalty_auto_mode”	1
“DAv3_gs_penalty_coef”	1
“DAv3_gs_penalty_inc_rate”	150
“DAv3_gs_max_penalty_coef”	0

References

- Agnetis, A., 2000. Scheduling no-wait robotic cells with two and three machines. *European Journal of Operational Research*. 123.2, 303–314. [https://doi.org/10.1016/S0377-2217\(99\)00258-1](https://doi.org/10.1016/S0377-2217(99)00258-1).
- Agnetis, A., Pacciarelli, D., 2000. Part sequencing in three-machine no-wait robotic cells. *Operations Research Letters*. 27.4, 185–192. [https://doi.org/10.1016/S0167-6377\(00\)00046-8](https://doi.org/10.1016/S0167-6377(00)00046-8).
- Albash, T., Lidar, D. A., 2018. Demonstration of a scaling advantage for a quantum annealer over simulated annealing. *Physical Review X*. 8.3, 031016. <https://doi.org/10.1103/PhysRevX.8.031016>.
- Alexeev, Y. *et al.*, 2021. Quantum computer systems for scientific discovery. *PRX Quantum*. 2.1, 017001. <https://doi.org/10.1103/PRXQuantum.2.017001>.
- Allahverdi, A., 2016. A survey of scheduling problems with no-wait in process. *European Journal of Operational Research*. 255.3, 665–686. <https://doi.org/10.1016/j.ejor.2016.05.036>.
- Aramon, M. *et al.*, 2019. Physics-inspired optimization for quadratic unconstrained problems using a digital annealer. *Frontiers in Physics*. 7, 48. <https://doi.org/10.3389/fphy.2019.00048>.
- Awasthi, A. *et al.*, 2016. GPGPU-based parallel algorithms for scheduling against due date, in: *2016 IEEE International Parallel and Distributed Processing Symposium Workshops*. 766–775. <https://doi.org/10.1109/IPDPSW.2016.66>.
- Awasthi, A. *et al.*, 2023. Quantum computing techniques for multi-knapsack problems. arXiv preprint 2301.05750. <https://doi.org/10.48550/ARXIV.2301.05750>.
- Blekos, K. *et al.*, 2023. A review on quantum approximate optimization algorithm and its variants. arXiv preprint 2306.09198. <https://doi.org/10.48550/ARXIV.2306.09198>.
- Bowman, E. H., 1959. The schedule-sequencing problem. *Operations Research*. 7.5, 621–624. <https://doi.org/10.1287/opre.7.5.621>.
- Brucker, P., 2007. *Scheduling Algorithms*. 5th ed. Springer-Verlag, Berlin, Heidelberg. <https://doi.org/10.1007/978-3-540-69516-5>.
- Brucker, P., Burke, E. K., Groenemeyer, S., 2012. A mixed integer programming model for the cyclic job-shop problem with transportation. *Discrete Applied Mathematics*. 160.13, 1924–1935. <https://doi.org/10.1016/j.dam.2012.04.001>.
- Cao, Y. *et al.*, 2019. Quantum chemistry in the age of quantum computing. *Chemical reviews*. 119.19, 10856–10915. <https://doi.org/10.1021/acs.chemrev.8b00803>.
- Carugno, C., Ferrari Dacrema, M., Cremonesi, P., 2022. Evaluating the job shop scheduling problem on a D-wave quantum annealer. *Scientific Reports*. 12.1, 6539. <https://doi.org/10.1038/s41598-022-10169-0>.
- Černý, V., 1985. Thermodynamical approach to the traveling salesman problem: an efficient simulation algorithm. *Journal of Optimization Theory and Applications*. 45.1, 41–51. <https://doi.org/10.1007/BF00940812>.
- Chakroun, I. *et al.*, 2013. Combining multi-core and gpu computing for solving combinatorial optimization problems. *Journal of Parallel and Distributed Computing*. 73.12, 1563–1577. <https://doi.org/10.1016/j.jpdc.2013.07.023>.
- D-Wave Systems Inc., 2020. D-Wave hybrid solver service: an overview. https://www.dwavesys.com/media/4bnpi53x/14-1039a-b_d-wave_hybrid_solver_service_an_overview.pdf. Last accessed 2022-11-08.
- Dawande, M. W. *et al.*, 2007. *Throughput optimization in robotic cells*. ISOR 101. Springer Science & Business Media. <https://doi.org/10.1007/0-387-70988-6>.

- Deutsch, D., Jozsa, R., 1992. Rapid solution of problems by quantum computation. *Proceedings of the Royal Society of London. Series A: Mathematical and Physical Sciences*. 439.1907, 553–558. <https://doi.org/10.1098/rspa.1992.0167>.
- Ebadi, S. *et al.*, 2022. Quantum optimization of maximum independent set using Rydberg atom arrays. *Science*. 376.6598, 1209–1215. <https://doi.org/10.1126/science.abo6587>.
- Farhi, E., Goldstone, J., Gutmann, S., 2014. A quantum approximate optimization algorithm. arXiv preprint 1411.4028. <https://doi.org/10.48550/ARXIV.1411.4028>.
- Feng, J., Che, A., 2013. Robotic cell cyclic scheduling considering cell layout, in: *Proceedings of the 32nd Chinese Control Conference*. 2622–2626. <https://ieeexplore.ieee.org/abstract/document/6639868>.
- Geitz, M. *et al.*, 2022. Solving the extended job shop scheduling problem with AGVs – classical and quantum approaches, in: P. Schaus (Ed.), *Integration of Constraint Programming, Artificial Intelligence, and Operations Research: 19th International Conference, (CPAIOR 2022), Proceedings*. LNCS 13292. Springer-Verlag, Los Angeles, CA, USA. 120–137. https://doi.org/10.1007/978-3-031-08011-1_10.
- Glover, F., Kochenberger, G., Du, Y., 2018. A tutorial on formulating and using QUBO models. arXiv preprint 1811.11538. <https://doi.org/10.48550/ARXIV.1811.11538>.
- Griva, I., Nash, S., Sofer, A., 2009. *Linear and Nonlinear Optimization: Second Edition*. Other Titles in Applied Mathematics. Society for Industrial, Applied Mathematics (SIAM, 3600 Market Street, Floor 6, Philadelphia, PA 19104).
- Grover, L. K., 1996. A fast quantum mechanical algorithm for database search, in: *Proceedings of the twenty-eighth annual ACM symposium on Theory of computing*. 212–219. <https://doi.org/10.1145/237814.237866>.
- Gurobi Optimization, LLC, 2023. Gurobi Optimizer Reference Manual. <https://www.gurobi.com>.
- Hall, N. G., Sriskandarajah, C., 1996. A survey of machine scheduling problems with blocking and no-wait in process. *Operations Research*. 44.3, 510–525. <https://doi.org/10.1287/opre.44.3.510>.
- IBM Quantum, 2023. Ibm quantum services. <https://quantum-computing.ibm.com>. Last accessed 2023-01-31.
- Ikeda, K., Nakamura, Y., Humble, T. S., 2019. Application of quantum annealing to nurse scheduling problem. *Scientific Reports*. 9, 12837. <https://doi.org/10.1038/s41598-019-49172-3>. arXiv: 1904.12139 [quant-ph].
- Jing, C., Huang, W., Tang, G., 2011. Minimizing total completion time for re-entrant flow shop scheduling problems. *Theoretical Computer Science*. 412.48, 6712–6719. <https://doi.org/10.1016/j.tcs.2011.08.030>.
- Kirkpatrick, S., Gelatt, C. D., Vecchi, M. P., 1983. Optimization by simulated annealing. *Science New Series*. 220.4598, 671–680. <https://doi.org/10.1126/science.220.4598.671>.
- Kochenberger, G. *et al.*, 2014. The unconstrained binary quadratic programming problem: a survey. *Journal of Combinatorial Optimization*. 28, 58–81. <https://doi.org/10.1007/s10878-014-9734-0>.
- Ku, W.-Y., Beck, J. C., 2016. Mixed integer programming models for job shop scheduling: a computational analysis. *Computers & Operations Research*. 73, 165–173. <https://doi.org/10.1016/j.cor.2016.04.006>.
- Li, Y. *et al.*, 2020. Quantum optimization and quantum learning: a survey. *IEEE Access*. 8, 23568–23593. <https://doi.org/10.1109/ACCESS.2020.2970105>.
- Liu, S. Q., Kozan, E., 2017. A hybrid metaheuristic algorithm to optimise a real-world robotic cell. *Computers & Operations Research*. 84, 188–194. <https://doi.org/10.1016/j.cor.2016.09.011>.

- Lobe, E., Lutz, A., 2022. Minor embedding in broken chimera and pegasus graphs is np-complete. arXiv preprint 2110.08325. <https://doi.org/10.48550/ARXIV.2110.08325>.
- Lucas, A., 2014. Ising formulations of many NP problems. *Frontiers in Physics*. 2, 5. <https://doi.org/10.3389/fphy.2014.00005>.
- Manne, A. S., 1960. On the job-shop scheduling problem. *Operations Research*. 8.2, 219–223. <https://doi.org/10.1287/opre.8.2.219>.
- Mizuno, Y., Komatsuzaki, T., 2023. Finding optimal pathways in chemical reaction networks using ising machines. arXiv preprint 2308.04544. <https://doi.org/10.48550/arXiv.2308.04544>.
- Nakayama, H. *et al.*, 2021. Description: third generation digital annealer technology. https://www.fujitsu.com/global/documents/about/research/techintro/3rd-g-da_en.pdf. Last accessed 2023-06-13.
- Nguyen, M.-T. *et al.*, 2023. Quantum optimization with arbitrary connectivity using rydberg atom arrays. *PRX Quantum*. 4.1, 010316. <https://doi.org/10.1103/PRXQuantum.4.010316>.
- Oshiyama, H., Ohzeki, M., 2022. Benchmark of quantum-inspired heuristic solvers for quadratic unconstrained binary optimization. *Scientific Reports*. 12.1. <https://doi.org/10.1038/s41598-022-06070-5>.
- Phillips, L. W., Unger, P. S., 1976. Mathematical programming solution of a hoist scheduling program. *AIIE Transactions*. 8.2, 219–225. <https://doi.org/10.1080/05695557608975070>.
- Pinedo, M. L., 2016. *Scheduling. Theory, Algorithms, and Systems*. 5th ed. Springer International. <https://doi.org/10.1007/978-3-319-26580-3>.
- Pritsker, A. A. B., Waiters, L. J., Wolfe, P. M., 1969. Multiproject scheduling with limited resources: a zero-one programming approach. *Management Science*. 16.1, 93–108. <https://doi.org/10.1287/mnsc.16.1.93>.
- Raymond, J. *et al.*, 2023. Hybrid quantum annealing for larger-than-QPU lattice-structured problems. *ACM Transactions on Quantum Computing*. 4.3, 1–30. <https://doi.org/10.1145/3579368>.
- Röck, H., 1984. Some new results in flow shop scheduling. *Zeitschrift für Operations Research*. 28.1, 1–16. <https://doi.org/10.1007/BF01919082>.
- Schuld, M., Sinayskiy, I., Petruccione, F., 2015. An introduction to quantum machine learning. *Contemporary Physics*. 56.2, 172–185. <https://doi.org/10.48550/arXiv.1409.3097>.
- Shabtay, D., Arviv, K., 2016. Optimal robot scheduling to minimize the makespan in a three-machine flow-shop environment with job-independent processing times. *Applied Mathematical Modelling*. 40.5, 4231–4247. <https://doi.org/10.1016/j.apm.2015.11.021>.
- Shor, P. W., 1994. Algorithms for quantum computation: discrete logarithms and factoring, in: *Proceedings 35th annual symposium on foundations of computer science*. IEEE. 124–134. <https://doi.org/10.1109/SFCS.1994.365700>.
- Steiner, G., Xue, Z., 2005. Scheduling in reentrant robotic cells: algorithms and complexity. *Journal of Scheduling*. 8.1, 25–48. <https://doi.org/10.1007/s10951-005-5314-6>.
- Stern, H. I., Vitner, G., 1990. Scheduling parts in a combined production-transportation work cell. *Journal of the Operational Research Society*. 41.7, 625–632. <https://doi.org/10.1057/jors.1990.86>.
- Streif, M. *et al.*, 2021. Beating classical heuristics for the binary paint shop problem with the quantum approximate optimization algorithm. *Physical Review A*. 104.1, 012403. <https://doi.org/10.1103/physreva.104.012403>.
- Tatsumura, K., Dixon, A. R., Goto, H., 2019. FPGA-based simulated bifurcation machine, in: *2019 29th International Conference on Field Programmable Logic and Applications (FPL)*. 59–66. <https://doi.org/10.1109/FPL.2019.00019>.

- Tomasiewicz, D. *et al.*, 2020. Foundations for workflow application scheduling on D-Wave system, in: *Computational Science–ICCS 2020*. Springer. 516–530. https://doi.org/10.1007/978-3-030-50433-5_40.
- Wagner, H. M., 1959. An integer linear-programming model for machine scheduling. *Naval Research Logistics Quarterly*. 6.2, 131–140. <https://doi.org/https://doi.org/10.1002/nav.3800060205>.
- Welch, B. L., 1947. The generalization of ‘Student’s’ problem when several different population variances are involved. *Biometrika*. 34.1–2, 28–35. <https://doi.org/10.1093/biomet/34.1-2.28>.
- Wurtz, J. *et al.*, 2023. Aquila: quera’s 256-qubit neutral-atom quantum computer. arXiv preprint 2306.11727. <https://doi.org/10.48550/arXiv.2306.11727>.
- Yarkoni, S. *et al.*, 2021. Multi-car paint shop optimization with quantum annealing, in: *2021 IEEE International Conference on Quantum Computing and Engineering (QCE)*. 35–41. <https://doi.org/10.1109/QCE52317.2021.00019>. arXiv: 2109.07876.
- Zbinden, S. *et al.*, 2020. Embedding algorithms for quantum annealers with chimera and pegasus connection topologies, in: P. Sadayappan *et al.* (Eds.), *High Performance Computing*. Springer International Publishing, Cham. 187–206. https://doi.org/10.1007/978-3-030-50743-5_10.